nature physics

ARTICLES

https://doi.org/10.1038/s41567-022-01726-5

Check for updates

OPEN

Flavour-selective localization in interacting lattice fermions

D. Tusi[1], L. Franchi[2], L. F. Livi[2], K. Baumann[3,4], D. Benedicto Orenes[5,6], L. Del Re[7], R. E. Barfknecht[5], T.-W. Zhou[2], M. Inguscio[1,5,8], G. Cappellini[1,5], M. Capone[3,9], J. Catani[1,5] and L. Fallani[1,2,5,10] ✉

A large repulsion between particles in a quantum system can lead to their localization, an effect responsible for the Mott insulator phases in strongly correlated materials. In a system with multiple orbitals, an orbital-selective Mott insulator can form, where electrons in some orbitals are predicted to localize while others remain itinerant. Here we demonstrate a more general version of this phenomenon by observing flavour-selective localization in an atom-based quantum simulator. Our experiment realizes Fermi–Hubbard models with an SU(3) symmetry that can be broken using a tunable coupling between flavours. We observe an enhancement of the localization associated with a selective Mott transition and the emergence of flavour-dependent correlations. Our realization of flavour-selective Mott physics demonstrates the potential of cold atoms to simulate interacting multicomponent materials such as superconductors and topological insulators.

Interactions shape the collective behaviour of many-particle quantum systems, leading to rich phase diagrams where conventional and novel phases can be induced by a controlled variation of external stimuli. The most direct example is perhaps the Mott insulator, where the large repulsion among particles leads to an insulating state despite the non-interacting system being a metal or a superfluid[1]. In solid-state physics, the interest in Mott insulators is reinforced by the observation that the proximity to a Mott transition is a horn of plenty where a variety of spectacular phases can be observed, high-temperature superconductivity[2,3] being only the tip of the iceberg[4].

In recent years, it has become clear that the standard SU(2) Fermi–Hubbard model is only one specific example, as many interesting materials require a description in terms of 'multicomponent' Hubbard models, for example when the conduction electrons have an additional orbital degree of freedom. These systems are not merely more complicated but rather host new phenomena, challenging the standard paradigm of Mott localization[5]. Indeed, when the symmetry between orbitals is broken, by some field or internal coupling, electrons in specific orbitals (or some combinations of them) can be Mott-localized while others remain itinerant, leading to surprising 'orbital-selective Mott insulators'[6].

Orbital-selective Mott physics has become a central concept for the description of a new class of high-T_c superconductors based on iron[7], as it can describe the anomalies of the metallic state[8–10] and the orbital character of superconductivity[11] in those systems. However, a clean observation of selective Mott transitions is intrinsically hard in solid-state systems because of the limited experimental control over the microscopic parameters and the orbital degree of freedom. The paradigm of selective Mott physics is itself far from being fully explored and has the potential to become a powerful framework to understand a variety of phenomena, from superconductivity to topological properties, in multicomponent quantum materials.

In this work, we take a broader perspective and treat orbital-selective Mott physics as an example of the general concept of flavour-selective Mott localization[12], which can be realized in a variety of multi-flavour systems, where the flavour can be the spin, the orbital or any other quantum number. We realize a minimal instance of this phenomenon by means of an atomic quantum simulator based on the optical manipulation of nuclear-spin mixtures of ultracold two-electron ^{173}Yb atoms. This platform allows the realization of multicomponent systems with global SU(N) interaction symmetry (where N is the number of components)[13,14], as in recent works reporting the realization of SU(N) quantum wires[15], SU(N) Mott insulators[16,17] and, more recently, SU(N) quantum magnetism[18]. Here, we introduce an approach to break the symmetry of SU(3) Fermi–Hubbard systems in a controlled way, which allows us to go beyond the investigations in the solid state and to observe directly the two key signatures of selective Mott physics[12]: an overall enhancement of Mott localization and the onset of flavour-selective correlations.

The experiment is performed with three-component ultracold ^{173}Yb Fermi gases with total atom number up to $N=4\times10^4$ and initial temperature $T\simeq0.2T_F$ (where T_F is the Fermi temperature for the single-component gas). The atoms are then trapped in a cubic three-dimensional (3D) optical lattice (lattice constant $d=\lambda/2=380\,\mathrm{nm}$), which realizes the multi-flavour Hubbard Hamiltonian

$$\hat{H} = -t\sum_{\langle i,j\rangle,\alpha}\left(\hat{c}^{\dagger}_{\alpha i}\hat{c}_{\alpha j}+\mathrm{h.c.}\right)+U\sum_{i,\alpha,\beta\neq\alpha}\hat{n}_{\alpha i}\hat{n}_{\beta i}+\hat{V}_{\mathrm{T}} +\frac{\Omega}{2}\sum_{i}\left(\hat{c}^{\dagger}_{1i}\hat{c}_{2i}+\mathrm{h.c.}\right) \quad (1)$$

where $\alpha,\beta\in\{1,2,3\}$ indicate the fermionic flavours (corresponding to nuclear spin states $m=+5/2$, $+1/2$ and $-5/2$, respectively), $\hat{c}^{\dagger}_{\alpha i}$ is the destruction operator for a fermion of flavour α in site i (h. c. denotes the Hermitian conjugate operator), $\hat{n}_{\alpha i}=\hat{c}^{\dagger}_{\alpha i}\hat{c}_{\alpha i}$ is the

[1]LENS European Laboratory for Nonlinear Spectroscopy, Sesto Fiorentino, Italy. [2]Department of Physics and Astronomy, University of Florence, Sesto Fiorentino, Italy. [3]SISSA Scuola Internazionale Superiore di Studi Avanzati, Trieste, Italy. [4]Laboratoire de Physique et Etude des Matériaux, UMR8213, CNRS/ESPCI/UPMC, Paris, France. [5]CNR-INO Istituto Nazionale di Ottica, Consiglio Nazionale delle Ricerche, Sesto Fiorentino, Italy. [6]ICFO - Institut de Ciències Fotòniques, The Barcelona Institute of Science and Technology, Castelldefels, Spain. [7]Department of Physics, Georgetown University, Washington, DC, USA. [8]Department of Engineering, Campus Bio-Medico University of Rome, Rome, Italy. [9]CNR-IOM Istituto Officina dei Materiali, Consiglio Nazionale delle Ricerche, Trieste, Italy. [10]INFN National Institute for Nuclear Physics, Florence, Italy. ✉e-mail: fallani@lens.unifi.it

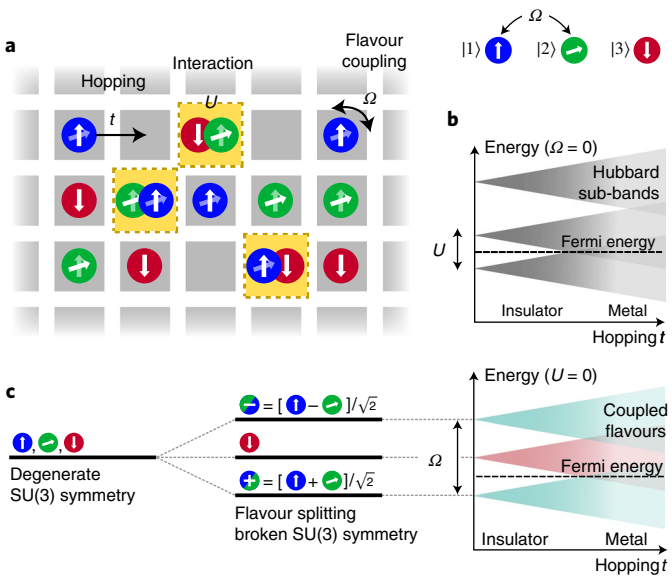

Fig. 1 | Sketch of the physical system. a, We consider a system of repulsively SU(3)-interacting fermions in a lattice. The global symmetry is broken by a coherent Rabi driving Ω between two internal states. **b**, In the absence of coupling, the system experiences a phase transition from an SU(3) metal to a Mott insulator as the hopping is reduced. **c**, The Rabi driving lifts the degeneracy between the states and, in a dressed basis picture, causes them to acquire different energies. The competition with the hopping can drive a transition from a metal to an insulator already in the non-interacting case. The energy band diagrams refer to the simplified case of a homogeneous system at a constant Fermi energy.

corresponding number operator, t is the tunnelling energy between nearest-neighbouring sites $\langle i,j\rangle$, U is the on-site repulsion energy between two atoms of different flavours and $\hat{V}_T = \kappa\sum_{i,\alpha} R_i^2 \hat{n}_{\alpha i}$ describes the effects of a slowly varying harmonic trapping potential (where R_i is the distance of site i from the trap centre and κ describes the strength of the trap). This last term determines the density in the lattice. In the non-interacting case ($U=0$) the average filling at $T=0$ and $\Omega=0$ can be calculated as ~1.8 atoms per site for the mean atom number of $N=2\times10^4$ considered in the experiments discussed below, while in the strongly interacting limit ($t=0$ and $\Omega=0$) it reduces to 1 atom per site (corresponding to the formation of Mott domains) (Supplementary Information). In the absence of the fourth term of equation (1), $\hat{H}$ has an intrinsic global SU(3) symmetry, which is ensured by the lack of variation of the atom–atom interactions with the spin state and by the realization of spin-independent optical potentials, that is, that U, t and κ do not depend on α. This symmetry is explicitly broken by the fourth term, which describes a coherent on-site coupling between flavours $|1\rangle$ and $|2\rangle$. This coupling is provided by a two-photon Raman process with a Rabi frequency of Ω/h (Supplementary Information) (where h is the Planck constant). At the single-particle level, this coupling lifts the degeneracy between the flavours, creating two dressed combinations $|\pm\rangle = (|1\rangle \pm |2\rangle)/\sqrt{2}$, energy-shifted from $|3\rangle$ by $\pm\Omega/2$, as sketched in Fig. 1c.

We use an adiabatic preparation sequence to produce an equilibrium state of the atomic mixture in the optical lattice, with equal state populations $N_1=N_2=N_3=N/3$ and in the presence of the coherent coupling Ω between states $|1\rangle$ and $|2\rangle$ (Supplementary Information). To characterize the degree of localization of the particles in the lattice, we measure the number of atoms N_d in doubly occupied sites (called 'doublons' in the following) with photoassociation spectroscopy, as in previous experiments that demonstrated the onset of Mott localization for ultracold fermions (refs. [16,19] and Supplementary Information). Figure 2a reports typical measurements of N_d as a function of the total atom number N. In a harmonically trapped system, the rate of change of N_d with respect to N provides information on the core compressibility[19,20]. A vanishing value of N_d over an extended range of N signals the presence of an incompressible state with one atom per site in the centre of the trap (since adding particles does not lead to a proportional increase of doublons), while the critical N above which N_d then departs from zero can be connected to the magnitude of the energy gap protecting the localized phase. Figure 2a shows two datasets for $U=2.6D$ (where $D=6t$ is the tunnelling energy times the lattice coordination number) and two different Rabi couplings $\Omega=0$ and $\Omega=1.6D$, respectively. A comparison between the two datasets clearly shows that the Rabi coupling Ω results in an enhanced suppression of doublons, enlarging the region of N where the incompressible state forms.

In the following, we take the doublon fraction $f_d=\langle N_d/N\rangle$, averaged over the N interval marked by the grey region in Fig. 2a as an indicator of the degree of Mott localization of the system. The measured values of f_d are shown as a function of U and Ω in Fig. 2b, clearly revealing the cooperative effect of Rabi coupling and repulsive interactions driving the system towards a Mott localized state. The same data are plotted with error bars in Fig. 2c,d along two different line cuts of the diagram in Fig. 2b. Figure 2c shows the effect of an increasing U in the transition towards an SU(3) Mott insulator for $\Omega=0$, while Fig. 2d shows a similar localization effect induced by Ω at a fixed interaction strength $U=2.6D$.

We now show a comparison of the experimental results with different theoretical analysis of the model in equation (1). Figure 3a shows a zero-temperature phase diagram obtained from dynamical mean-field theory (DMFT)[21] for the homogeneous system ($V_T=0$) with a uniform 1/3 filling (one atom per site) and an equal number of particles for each flavour. The phase diagram clearly has the same shape as the experimental one, showing that the Hubbard U and the coupling Ω cooperate in driving the system from a metallic phase to a more localized state. Between the standard metal and the Mott phase, we find a region where the degree of correlations (as measured by the quasiparticle weight) is strongly selective, the coupled flavours being much more localized than the uncoupled one. It is evident that both selective and global Mott localization occur at a smaller U if Ω is included.

To connect this effect to the experimentally measured signal, Fig. 3b shows the doublon fraction f_d obtained from the homogeneous DMFT results after a local density approximation (LDA) analysis, to take into account the effect of the harmonic trapping in V_T. The reduction of f_d with increasing Ω is in agreement with the experimental observations reported in Fig. 2. The lack of a quantitative matching with Fig. 2d can be attributed to imperfections in the initial state preparation and to the finite temperature of the experiment, resulting in an average entropy per particle of $S/N\approx2.5k_B$ (where k_B is the Boltzmann constant), which is known[20] to produce an effect on the double occupancies in a trapped system already at $\Omega=0$. A comprehensive analysis of finite-temperature effects is presented in the Supplementary Information, showing that thermal fluctuations do explain the discrepancy between experiments and theory, without spoiling the properties of the expected zero-temperature phases. There we also show experimental evidence that the entropy of the system is not appreciably affected by the presence of the Raman coupling, ruling out unwanted heating as a possible cause for the reduction of f_d.

Finally, Fig. 3c shows the result of a zero-temperature DMRG calculation of f_d for a harmonically trapped one-dimensional (1D) system (Supplementary Information). Although quantitative agreement with the experimental data should not be sought (because of the different dimensionality and the finite temperature of the experimental realization), the overall behaviour, that is, a reduction

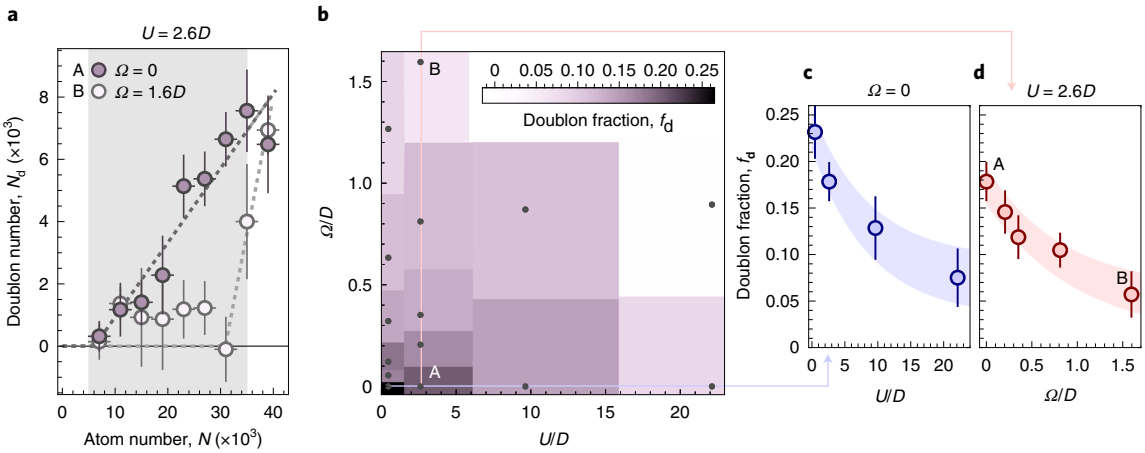

Fig. 2 | Measurement of double occupancies. a, Number of atoms in doubly occupied sites N_d as a function of the total atom number N for two different values of Ω and the same $U=2.6D$. **b**, Average doublon fraction f_d as a function of U/D and Ω/D. The actual measurements are marked by the points. **c**,**d**, Subsets of the data for two different cross sections of the plot in **b**, that is, for $\Omega=0$ (**c**) and for $U=2.6D$ (**d**). The measurements in **b**–**d** are averages over an interval $N=(5\text{–}35)\times10^3$. Error bars in **a**, **c** and **d** are obtained by a bootstrap analysis (Supplementary Information). Dashed lines in **a** are fits with a piecewise function (null + straight line), while colour shades in **c** and **d** are guides to the eye representing the experimental uncertainty.

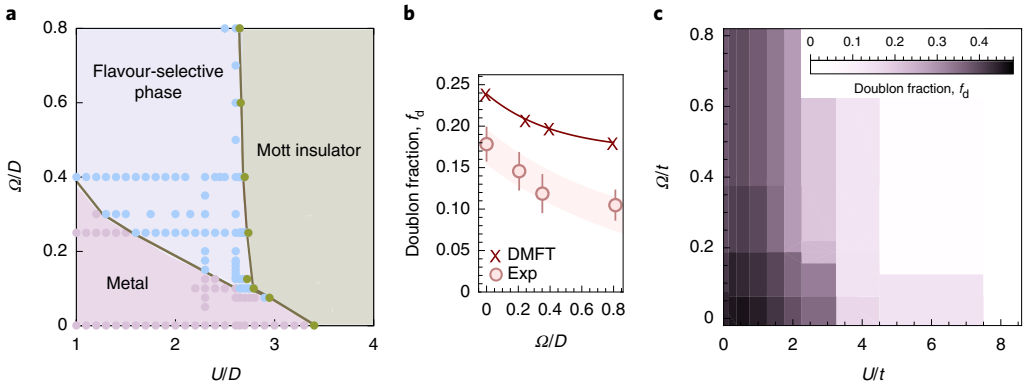

Fig. 3 | Theoretical analysis. a, DMFT phase diagram for a homogeneous system at $T=0$ and 1/3 filling. The points refer to different parameter runs. The boundary between the standard metal and the region of selective correlations marks a sharp crossover where the quasiparticle weight of the coupled flavours drops rapidly to a value smaller than 0.05. **b**, The crosses show the doublon fraction for the trapped system at $U=2.6D$ and different Ω/D, obtained from a LDA analysis of the homogeneous DMFT results with the experimental parameters. The points are the experimental data of Fig. 2d (averaging procedure and error bars are explained in the caption of that figure). **c**, Doublon fraction obtained from DMRG for a 1D trapped system of $N=21$ particles at $T=0$.

of the doublons for increasing U and Ω, is correctly captured and agrees also with DMFT. This also indicates that the phenomena we are exploring are generic and qualitatively independent from the dimensionality.

In addition to the enhancement of the Mott localization, the DMFT phase diagram of Fig. 3a shows that Ω is expected to result in a flavour-dependent localization of the many-body system. The flavour-selective behaviour can be detected experimentally by resolving the spin character of the doublons, that is, by counting how many atoms form doublons in each of the three pairs $|12\rangle$, $|23\rangle$ and $|31\rangle$ by means of state-selective photoassociation at a high magnetic field (Supplementary Information). Figure 4 shows the quantity $\gamma(12)=N_d(12)/N_d$, where $N_d(12)$ is the number of atoms forming doublons in the $|12\rangle$ channel, as a function of Ω and fixed $U=2.6D$. The measured value at $\Omega=0$ agrees with the expectation for a system with SU(3) symmetry, for which $\gamma(12)=1/3$. As Ω is increased and the SU(3) symmetry is broken, $\gamma(12)$ diminishes, eventually approaching zero for $\Omega\approx D$. The doublons acquire a strongly flavour-selective behaviour.

This suppression of $|12\rangle$ doublons is triggered by the polarization effect in the rotated $|\pm\rangle$ basis, which can be understood, at a qualitative level, already from the simplified, non-interacting case sketched in Fig. 1c. While $|23\rangle$ and $|31\rangle$ doublons can be formed by two fermions in the lowest single-particle states $|+\rangle$ and $|3\rangle$, $|12\rangle$ doublons can be formed only if the two fermions occupy states $|+\rangle$ and $|-\rangle$, therefore with an additional energy cost of $\Omega/2$. Interactions then increase this effect[12], leading to strong flavour-selective results even for small values of Ω.

The crosses in Fig. 4 are the result of a DMFT calculation in which the flavour populations are kept equal and the harmonic trapping V_T has been taken into account in an LDA approach. The results of this numerical calculation are in good agreement with the experimental findings, with a larger degree of selectivity for the theoretical calculation. We argue that better agreement could be sought by including finite-temperature effects in the calculation. Indeed, we expect the state-selective behaviour to be reduced by the thermal occupation of higher-energy states, leading to an effective reduction of the polarization in the $|+\rangle$, $|-\rangle$ basis.

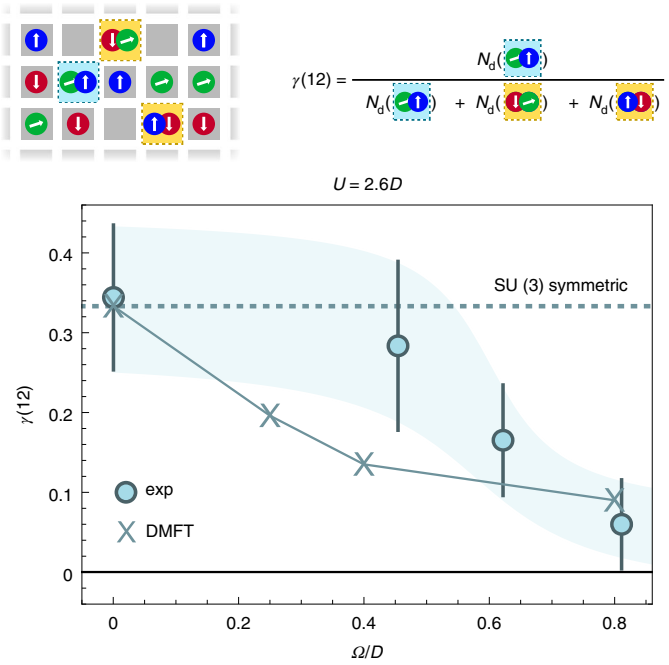

Fig. 4 | Evidence of state-selective correlations. Experimental values of $\gamma(12)$ as a function of Ω/D for a fixed $U=2.6D$. The circles are averages over an interval $N=(5\text{–}35)\times10^3$, error bars are obtained from a bootstrap analysis (Supplementary Information) while the colour shade is a guide to the eye. The crosses are obtained from an LDA analysis of the DMFT results. The dashed line shows the expected value for a system with SU(3) symmetry.

Note that the experimental observation of a finite number of $|12\rangle$ doublons at small but finite Ω is an indication of the validity of the protocol used for the preparation of the atomic state, which is different for $\Omega=0$ and $\Omega>0$ (Supplementary Information). Note also that, despite the polarization in the dressed $|+\rangle$, $|-\rangle$ basis discussed above, we have verified that the populations of the bare states $|1\rangle$, $|2\rangle$ and $|3\rangle$ remain always equal under all the experimental conditions we have considered. This is indeed an important aspect of our experiment. If the populations of the bare states were not fixed (and in particular if N_3 was left free to adapt), the dressed states would be populated according to the scheme in Fig. 1c, leading to $N_1=N_2>N_3$, which favours flavour-selective physics already in the non-interacting system. The experimental state preparation procedure counteracts the trivial differentiation between flavours by forcing an even occupation. Therefore, we conclude that the flavour selectivity that we observed is essentially due to quantum correlations induced by interactions.

In the theoretical DMFT calculations, the equal population constraint is enforced by including an external field h (Supplementary Information) that favours the occupation of $|3\rangle$ in such a way as to match the experimental condition $N_1+N_2+N_3=N/3$. Comparing with ref. [12], where the populations were left free, we observe that the quantum correlations leading to the selective regime survive the inclusion of the field h. In general terms, single-particle effects trigger flavour selectivity, but the inclusion of interactions strongly enhances the differentiation, turning a minor modulation of kinetic energy into a quantitative phenomenon which can also lead to a selective Mott transition[22]. This is a very general framework, underlying many investigations of multicomponent models.

Exploiting an idealized quantum simulator, we have obtained clear-cut evidence for correlation-induced flavour-selective physics, where the SU(N) symmetry-breaking coupling Ω is only the trigger of a flavour-selective phenomenon which is fundamentally driven by correlation effects. Our realization of multicomponent Hubbard physics with coherent internal couplings opens new paths for the quantum simulation of new classes of materials ranging from high-temperature superconductors to interacting topological insulators as described by the Bernevig–Hughes–Zhang model[23]. Once the coupling is realized with a non-zero momentum transfer (that is, non-collinear Raman beams), a full range of possibilities will emerge, including the study of magnetic crystals[24], fractional quantum Hall states[25] and the effect of interactions of topological phase transitions[26] and on the associated edge states[27].

Online content

Any methods, additional references, Nature Research reporting summaries, source data, extended data, supplementary information, acknowledgements, peer review information; details of author contributions and competing interests; and statements of data and code availability are available at https://doi.org/10.1038/s41567-022-01726-5.

Received: 20 May 2021; Accepted: 15 July 2022;
Published online: 22 September 2022

References

1. Mott, N. F. The basis of the electron theory of metals, with special reference to the transition metals. *Proc. Phys. Soc. Lond. A* **62**, 416 (1949).
2. Anderson, P. W. The resonating valence bond state in La_2CuO_4 and superconductivity. *Science* **235**, 1196–1198 (1987).
3. Lee, P. A., Nagaosa, N. & Wen, X.-G. Doping a Mott insulator: physics of high-temperature superconductivity. *Rev. Mod. Phys.* **78**, 17–85 (2006).
4. Paschen, S. & Si, Q. Quantum phases driven by strong correlations. *Nat. Rev. Phys.* **3**, 9–26 (2021).
5. Georges, A., de' Medici, L. & Mravlje, J. Strong electronic correlations from Hund's coupling. Annu. Rev. *Condens. Matter Phys.* **4**, 137–178 (2013).
6. Vojta, M. Orbital-selective Mott transitions: heavy fermions and beyond. *J. Low. Temp. Phys.* **161**, 203–232 (2010).
7. Kamihara, Y., Watanabe, T., Hirano, M. & Hosono, H. Iron-based layered superconductor $La[O_{1-x}F_x]FeAs$ ($x=0.05$–0.12) with $T_c=26$ K. *J. Am. Chem. Soc.* **130**, 3296–3297 (2008).
8. de' Medici, L., Giovannetti, G. & Capone, M. Selective Mott physics as a key to iron superconductors. *Phys. Rev. Lett.* **112**, 177001 (2014).
9. Kostin, A. et al. Imaging orbital-selective quasiparticles in the Hund's metal state of FeSe. *Nat. Mater.* **17**, 869–874 (2018).
10. Capone, M. Orbital-selective metals. *Nat. Mater.* **17**, 855–856 (2018).
11. Sprau, P. O. et al. Discovery of orbital-selective Cooper pairing in FeSe. *Science* **357**, 75–80 (2017).
12. Del Re, L. & Capone, M. Selective insulators and anomalous responses in three-component fermionic gases with broken SU(3) symmetry. *Phys. Rev. A* **98**, 063628 (2018).
13. Gorshkov, A. V. et al. Two-orbital SU(N) magnetism with ultracold alkaline-earth atoms. *Nat. Phys.* **6**, 289–295 (2010).
14. Cazalilla, M. A. & Rey, A. M. Ultracold Fermi gases with emergent SU(N) symmetry. *Rep. Prog. Phys.* **77**, 124401 (2014).
15. Pagano, G. et al. A one-dimensional liquid of fermions with tunable spin. *Nat. Phys.* **10**, 198–201 (2014).
16. Taie, S., Yamazaki, R., Sugawa, S. & Takahashi, Y. An SU(6) Mott insulator of an atomic Fermi gas realized by large-spin Pomeranchuk cooling. *Nat. Phys.* **8**, 825–830 (2012).
17. Hofrichter, C. et al. Direct probing of the Mott crossover in the SU(N) Fermi–Hubbard model. *Phys. Rev. X* **6**, 021030 (2016).
18. Ozawa, H., Taie, S., Takasu, Y. & Takahashi, Y. Antiferromagnetic spin correlation of SU(N) Fermi gas in an optical superlattice. *Phys. Rev. Lett.* **121**, 225303 (2018).
19. Jördens, R., Strohmaier, N., Günter, K., Moritz, H. & Esslinger, T. A Mott insulator of fermionic atoms in an optical lattice. *Nature* **455**, 204–207 (2008).
20. Jördens, R. et al. Quantitative determination of temperature in the approach to magnetic order of ultracold fermions in an optical lattice. *Phys. Rev. Lett.* **104**, 180401 (2010).
21. Georges, A., Kotliar, G., Krauth, W. & Rozenberg, M. J. Dynamical mean-field theory of strongly correlated fermion systems and the limit of infinite dimensions. *Rev. Mod. Phys.* **68**, 13–125 (1996).
22. de' Medici, L., Hassan, S. R., Capone, M. & Dai, X. Orbital-selective Mott transition out of band degeneracy lifting. *Phys. Rev. Lett.* **102**, 126401 (2009).

23. Bernevig, B. A., Hughes, T. L. & Zhang, S.-C. Quantum spin Hall effect and topological phase transition in HgTe quantum wells. *Science* **314**, 1757–1761 (2006).
24. Barbarino, S., Taddia, L., Rossini, D., Mazza, L. & Fazio, R. Magnetic crystals and helical liquids in alkaline-earth fermionic gases. *Nat. Commun.* **6**, 8134 (2015).
25. Calvanese Strinati, M. et al. Laughlin-like states in bosonic and fermionic atomic synthetic ladders. *Phys. Rev. X* **7**, 021033 (2017).
26. Amaricci, A., Budich, J. C., Capone, M., Trauzettel, B. & Sangiovanni, G. First-order character and observable signatures of topological quantum phase transitions. *Phys. Rev. Lett.* **114**, 185701 (2015).
27. Amaricci, A. et al. Edge state reconstruction from strong correlations in quantum spin Hall insulators. *Phys. Rev. B* **95**, 205120 (2017).
28. Tusi, D. et al. Datasets for 'Flavour-selective localization in interacting lattice fermions'. *Zenodo* https://doi.org/10.5281/zenodo.6608992 (2022).

Data availability

All the experimental and theoretical data presented in the figures of the main article are available for download from an open repository[28]. Additional information is available from the corresponding author upon reasonable request. Source data are provided with this paper.

Code availability

The numerical codes used in the current study are available from the corresponding author upon reasonable request.

Acknowledgements

We acknowledge insightful discussions with M. Dalmonte, D. Clément and F. Scazza and financial support from projects TOPSIM ERC consolidator grant no. 682629, QTFLAG QuantERA ERA-NET Cofund in Quantum Technologies, TOPSPACE MIUR FARE project, MIUR PRIN project 2017E44HRF, MIUR PRIN project 2015C5SEJJ, MIUR PRIN project 20172H2SC4 and INFN FISh project. L.D.R. was supported by the U.S. Department of Energy, Office of Science, Basic Energy Sciences, Division of Materials Sciences and Engineering under grant no. DE-SC0019469.

Author contributions

L.Fa., J.C. and M.C. conceived the experiments. D.T., L.F.L., L.Fr., D.B.O. and G.C. carried out the measurements. L.Fa., L.F.L., L.Fr. and D.T. analysed the experimental results. K.B., L.D.R. and M.C. performed DMFT calculations. R.E.B. performed DMRG calculations. L.F.L. and L.Fa. performed exact diagonalization calculations. All authors contributed extensively to the discussion of the results and to the writing of the manuscript.

Competing interests

The authors declare no competing interests.

Additional information

Supplementary information The online version contains supplementary material available at https://doi.org/10.1038/s41567-022-01726-5.

Correspondence and requests for materials should be addressed to L. Fallani.

Peer review information *Nature Physics* thanks the anonymous reviewers for their contribution to the peer review of this work

Reprints and permissions information is available at www.nature.com/reprints.